

Independent freezing of charge and spin dynamics in $\text{La}_{1.5}\text{Sr}_{0.5}\text{CoO}_4$.

I. A. Zaliznyak¹, J. P. Hill¹, J. M. Tranquada¹, R. Erwin², Y. Moritomo³

¹*Department of Physics, Brookhaven National Laboratory, Upton, New York 11973-5000*

²*National Institute of Standards and Technology, Gaithersburg, Maryland 20899*

³*Center for Integrated Research in Science and Engineering (CIRSE) and Department of Applied Physics, Nagoya University, Nagoya 464-01, Japan
(November 17, 2018)*

We present elastic and quasielastic neutron scattering measurements characterizing peculiar short-range charge-orbital and spin order in the layered perovskite material $\text{La}_{1.5}\text{Sr}_{0.5}\text{CoO}_4$. We find that below $T_c \approx 750$ K holes introduced by Sr doping lose mobility and enter a statically ordered *charge glass* phase with loosely correlated checkerboard arrangement of empty and occupied $d_{3z^2-r^2}$ orbitals (Co^{3+} and Co^{2+}). The dynamics of the resultant mixed spin system is governed by the anisotropic nature of the crystal-field Hamiltonian and the peculiar exchange pattern produced by the orbital order. It undergoes a *spin freezing* transition at much a lower temperature, $T_s \lesssim 30$ K.

PACS numbers: 71.28.+d 71.45.Lr 75.10.-b, 75.40.Gb, 75.50.Ee

The instability of the doped transition-metal oxides towards formation of cooperative charge and spin ordered phases is one of the central phenomena in the physics of colossal magnetoresistance (CMR) materials and high temperature superconductors. Charge segregation into lines [1] which separate stripes of antiphase antiferromagnetic domains in $\text{La}_{2-x}\text{Sr}_x\text{CuO}_{4+y}$ (LSCO) cuprates at small x , is, according to some theories, key to their superconductivity [2]. In perovskite manganates, built of essentially isostructural Mn-O layers [3], doping first destroys the cooperative Jahn-Teller (JT) distortion of the orbitally-ordered insulating state [4], and induces a transition to a ferromagnetic metal (FM) [5]. The extremely strong response of transport properties in the FM phase to an applied magnetic field, termed CMR, results from the strong Hund's coupling of charge carriers to the Mn^{4+} core spins [6]. Then, at doping $x \approx 0.5$ an instability towards another kind of charge-orbital order, with a checkerboard arrangement of $\text{Mn}^{3+}/\text{Mn}^{4+}$ ions, results in an antiferromagnetic (AFM) insulating ground state. This doping level is argued to be of greatest technological relevance [3], since at half-doping transport properties usually show the strongest response to a magnetic field. To understand the physics of charge/spin ordered (CO/SO) phases, and, in particular, to answer the question of whether CO/SO are independent instabilities or closely coupled, the relative importance of the various interactions (superexchange, double exchange, Coulomb repulsion, JT distortion) needs to be clarified. Experimentally this can be done by studying different compounds in which the strengths of the above interactions vary.

The first complete characterization of the spin and charge order in the half-doped regime by means of neutron diffraction was reported for $\text{La}_{1.5}\text{Sr}_{0.5}\text{MnO}_4$ [7]. Nuclear scattering accompanying the CO was found below $T_{co} \approx 217$ K, where the steep rise in resistivity manifests the transition to an insulating state. A magnetic signal consistent with simple collinear antiferromagnetic

(AFM) order appeared below $T_{so} \approx 110$ K. CO was confirmed in a recent X-ray resonant scattering experiment [8], which has also provided the first direct evidence of the concomitant orbital order (OO). Similar charge, orbital and magnetic order was also observed in the ground state of half-doped pseudocubic manganates [9]. In most cases, the charge orders at a somewhat higher temperature than the spins do, but whether the CO instability occurs independently or is driven by the magnetic/orbital fluctuations is a topic of continuing debate [10,11].

Here we report a detailed neutron scattering study of the closely related layered cobalt oxide $\text{La}_{1.5}\text{Sr}_{0.5}\text{CoO}_4$. We argue that strong single-ion anisotropy, mediated by the relativistic spin-orbit coupling usually neglected in cuprates and manganates, effectively decouples charge ordering from low-energy spin fluctuations. This is reflected in the spectacular difference in CO and SO transition temperatures, $T_{co}/T_{so} \gtrsim 20$ in this material. In fact, strong planar anisotropy leads to a *quenching of the spin angular momentum* on the Co^{3+} sites, in full analogy with the well-known quenching of the orbital momentum by the crystal field. Combined with the checkerboard arrangement of the doped holes in the CoO_2 planes this makes the spin system of $\text{La}_{1.5}\text{Sr}_{0.5}\text{CoO}_4$ a strongly frustrated square lattice antiferromagnet.

Electronic configurations of Co^{2+} ($3d^7$) and Co^{3+} ($3d^6$) ions are related to those of Mn^{4+} and Mn^{3+} , respectively, by virtue of electron-hole symmetry. However, in the case of cobalt, Hund's rule is in close competition with the cubic crystal field, the latter splitting the $3d$ level into a lower-lying t_{2g} triplet and an e_g doublet of $d_{x^2-y^2}$ and $d_{3z^2-r^2}$ orbitals. As a result, even though Co^{2+} is in the high-spin state ($t_{2g}^5 e_g^2$, $S=3/2$), Co^{3+} obtained by adding the fourth hole may be either in the high $t_{2g}^4 e_g^2$ (HS, $S=2$), intermediate $t_{2g}^5 e_g^1$ (IS, $S=1$), or low spin state t_{2g}^6 (LS, $S=0$) [13]. Transitions between different spin states are not uncommon in Co compounds. If LS is the ground state, a decrease in free energy due to the higher mag-

netic entropy may drive transitions to IS and HS states with increasing temperature, as observed in LaCoO_3 [14]. For the purpose of the present study, however, the spin state of the Co^{3+} ions is not important at sufficiently low temperatures where spin order occurs. Indeed, *any integer spin will be frozen in a singlet state* by strong planar anisotropy, rendering ions effectively non-magnetic for low-energy fluctuations [12].

We studied a piece (0.48 g) of high quality single crystal of $\text{La}_{1.5}\text{Sr}_{0.5}\text{CoO}_4$ grown by the floating-zone method [13]. In the temperature range $6\text{ K} \lesssim T \lesssim 600\text{ K}$ covered in our experiment, the crystal remained in the tetragonal “HTT” phase (space group $I4/mmm$), with low T lattice parameters $a = 3.83\text{ \AA}$ and $c = 12.5\text{ \AA}$. However, to index the superlattice peaks it is convenient to choose a unit cell that is twice as large ($\sqrt{2}a \times \sqrt{2}a \times c$) corresponding to space group $F4/mmm$.

Most of the experiments were performed on the BT2 and BT4 3-axis thermal neutron spectrometers at the NIST Center for Neutron Research. Some preliminary measurements were done on the H8 spectrometer at the High Flux Beam Reactor at Brookhaven. In all cases, PG(002) reflections were used at the monochromator and analyser, supplemented by PG filters to suppress the higher-order contamination. The energy of the scattered neutrons was fixed at $E_f = 14.7\text{ meV}$. Beam collimations before the monochromator and after the analyser were kept at $\approx 60'$ and $\approx 100'$, respectively, while around the sample they were set either to $20' - 20'$ or to $42' - 62'$ depending on the resolution required. Our sample is a cylinder with axis parallel to $[010]$ direction, $D \approx 4\text{ mm}$, $L \approx 3\text{ mm}$. It was mounted in the displax refrigerator with axis vertical, allowing wavevector transfers in the $(h0l)$ reciprocal lattice plane. Rocking curves about the $[010]$ direction reveal a mosaic broadening of less than 0.25° . Normalization of the scattered intensity was done using the incoherent scattering from a vanadium sample.

Figure 1 shows a survey of the low-temperature elastic scattering in $\text{La}_{1.5}\text{Sr}_{0.5}\text{CoO}_4$. Peaks of magnetic and structural origin are easily distinguished by their characteristic wavevector dependences. The magnetic intensity is proportional to the Fourier-transform of the density of unpaired electrons (the magnetic form factor) squared, $|f(Q)|^2$, which becomes weaker at large Q , while the intensity from small nuclear displacements increases as $\sim Q^2$. This leads us to conclude that the peaks in Fig. 1(b), centered at slightly incommensurate positions $\tau \pm \mathbf{Q}_m$, $\mathbf{Q}_m = (0.5 + \epsilon, 0, 1)$ with $\epsilon \approx 0.017$, are magnetic, while stronger feature in Fig. 1(c) and features in Fig. 1(d) result from the modulations of the atomic positions accompanying the charge order of $\text{Co}^{2+}/\text{Co}^{3+}$ ions. None of the superstructure peaks are resolution-limited in Q , indicating finite-range *correlated glass* type modulations. They are static on the time scale $\delta t \lesssim 1\text{ ps}$ as determined by the energy resolution of our experiment. The diffuse nature of the scattering is most apparent in

scans along the \mathbf{c}^* ($[001]$) direction, which reflects the anisotropy of the correlation lengths: in-plane correlations are much better developed than inter-plane (see Table 1).

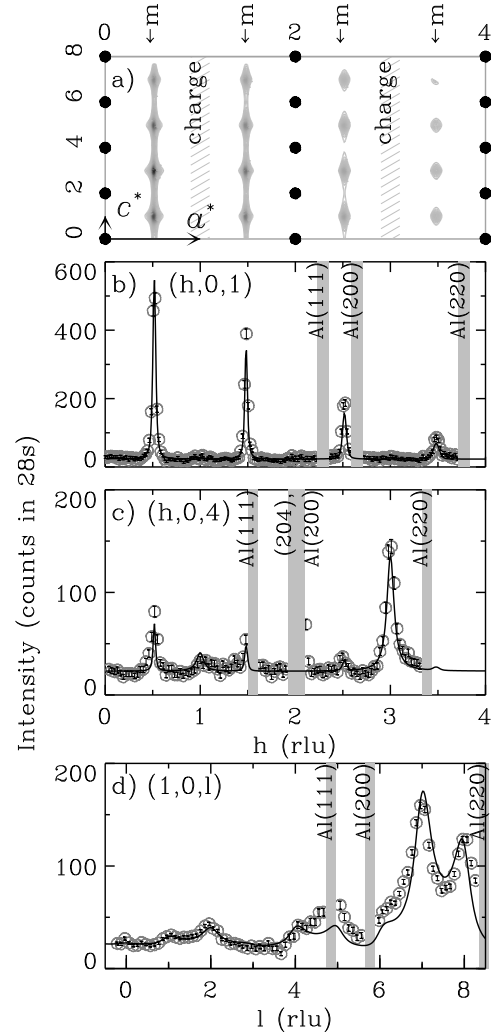


FIG. 1. Survey of the elastic scattering in the $(h0l)$ reciprocal plane of $\text{La}_{1.5}\text{Sr}_{0.5}\text{CoO}_4$. (a) Solid circles show allowed nuclear Bragg reflections, hatched areas mark regions where additional nuclear scattering due to the charge order is observed. The grey-scale map represents calculated magnetic intensity. (b)-(d) representative scans through the peaks of magnetic and charge-orbital scattering collected at $T = 10\text{ K}$ (b) and $T = 6.1\text{ K}$ (c),(d). Points in grey-shaded regions contaminated with aluminum scattering are removed. Solid curves show the fits discussed in text.

The incommensurability of the charge-order peaks, if any, is too small to be directly resolved, because of the short correlation length and the overlap of peaks at $\tau \pm \mathbf{Q}_c$. However, the scattering is consistent with the modulation wave vectors $\mathbf{Q}_c = (1 + 2\epsilon, 0, l)$ and $(0, 1 + 2\epsilon, l)$, with $l = 0$ or 1 . If ϵ is zero, the charge order corresponds to a checkerboard superstructure within each CoO_2 plane, as indicated in Fig. 2(c). The magnetic

modulation corresponds to almost antiferromagnetic order on either the Co^{2+} or Co^{3+} sublattice, with a superposed long-wavelength modulation along **a** (or **b**).

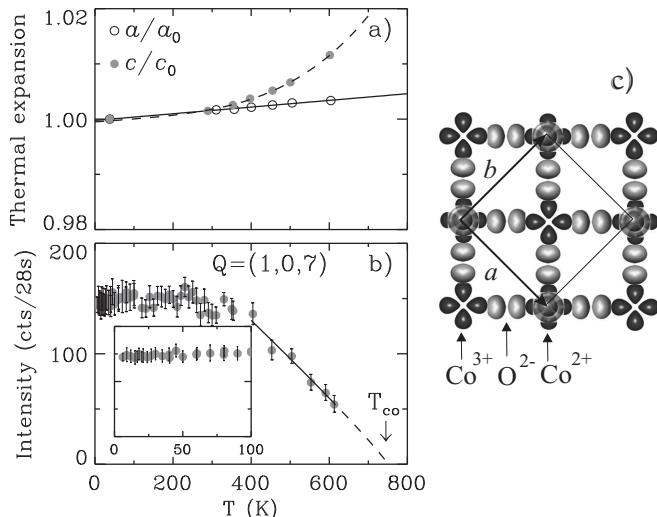


FIG. 2. (a) Relative change in the in-plane (open) and inter-plane (closed symbols) lattice spacings refined in the longitudinal scans through (200) and (006) Bragg reflections. (b) Temperature dependence of the intensity of the diffuse peak at $\mathbf{Q} = (107)$ associated with the checkerboard charge-orbital order. Insert expands the low- T region, $T \leq 100$ K. (c) Schematic drawing of Co-O bonding orbitals and checkerboard order of $\text{Co}^{2+}/\text{Co}^{3+}$ valence in $a-b$ plane.

For the quantitative analysis of nuclear scattering accompanying the charge order, we use the following correlation function between the displacement $\varepsilon_{\mu\mathbf{r}}$ of atom μ at the lattice point $\mathbf{r} = r_a\hat{\mathbf{a}} + r_b\hat{\mathbf{b}} + r_c\hat{\mathbf{c}}$ and $\varepsilon_{\mu'\mathbf{0}}$ of atom μ' at $\mathbf{0}$:

$$\langle \varepsilon_{\mu\mathbf{r}}^\alpha \varepsilon_{\mu'\mathbf{0}}^\beta \rangle = \varepsilon_\mu^\alpha \varepsilon_{\mu'}^\beta \cos(\mathbf{Q}_c \mathbf{r}) e^{-(|r_a|+|r_b|)/\xi_{\parallel}^{co}-|r_c|/\xi_{\perp}^{co}}, \quad (1)$$

describing a short-range harmonic modulation. Brackets denote an average over the crystal volume; $\alpha, \beta = x, y, z$; and ξ_{\parallel}^{co} and ξ_{\perp}^{co} are the charge-order correlation lengths parallel and perpendicular to the planes, respectively. The scattering cross-section obtained from Eq. (1) upon appropriate Fourier transformation has the form of factorized “lattice Lorentzians” [15] in three directions, weighted with $\left| \sum_{\mu} (\mathbf{Q} \cdot \varepsilon_{\mu}) b_{\mu} e^{-i\mathbf{Q} \cdot \mathbf{r}_{\mu}} \right|^2$, similar to that used to describe finite-range stripe correlations in LSCO [1]. Here b_{μ} is the scattering length (including the Debye-Waller factor) of the nucleus at position \mathbf{r}_{μ} in the unit cell. The Q -dependence of the structural diffuse intensity evident in scans along \mathbf{c}^* , Fig 1(d), suggests that it arises from breathing-type distortions of the oxygen octahedra surrounding the Co ions. Indeed, it appears sufficient to consider displacements of the in-plane oxygens O(1), $\varepsilon_{O(1)}^{x,y}$, and apical oxygens O(2), $\varepsilon_{O(2)}^z$, along the corresponding Co-O bonds, to obtain a good description of the observed “charge” scattering. Solid curves in Fig. 1(c),(d) present the neutron intensity calculated

from Eq. (1) after appropriate normalization and correction for the spectrometer resolution. The parameters $\varepsilon_{O(1)}^{x,y} = 0.042(4)$ Å, $\varepsilon_{O(2)}^z = -0.066(2)$ Å, and the correlation lengths shown in Table 1 were obtained in a global fit of all scans around $\tau \pm \mathbf{Q}_c$. The error bars shown do not include any possible systematic error from the vanadium normalization, which relied upon a knowledge of the vertical beam divergences (note the absence of arbitrary scaling factors between calculated and measured intensities in all panels of Fig. 1).

Figure 2 shows the temperature dependence of the peak intensity of the diffuse “charge” scattering and lattice thermal expansion in the **a** and **c** directions. Although we could not reach the CO melting temperature, an estimate of $T_{co} \approx 750$ K is obtained by extrapolation shown in Fig. 2(b). Strong nonlinear decrease of the c lattice spacing which accompanies the charge order is indirect evidence of the concomitant *orbital order*. This is because the checkerboard ordering of empty and occupied out-of-plane $d_{3z^2-r^2}$ orbitals, combined with the body-centered stacking of Co-O planes, $\delta = [\frac{1}{2}0\frac{1}{2}]$, allows a reduction of the inter-plane spacing.

We analyze the magnetic scattering cross section starting from a spin-spin correlation function similar to Eq. (1). By simultaneously fitting all of the magnetic peaks measured at $T = 10(3)$ K, we obtain a SO incommensurability $\epsilon = 0.017(1)$ and the correlation lengths shown in Table 1. We also find that the spin structure is planar, and isotropic within the $a-b$ plane. This agrees with the static susceptibility data [13], which yield an estimated $D \gtrsim 400$ K for the XY-type anisotropy energy. For $T \ll D$ this restricts any integer spin to a singlet state [12]. Further support for the conclusion that Co^{3+} ions are effectively non-magnetic is provided by small value of the frozen magnetic moment, $\langle \mu \rangle = 1.4(1)\mu_B$ per Co site refined for a single domain model. Assuming two equivalent \mathbf{Q}_m domains with half of the sites occupied by magnetic Co^{2+} ions, we obtain $\mu_{\text{Co}^{2+}} \approx 2.9\mu_B$, within 20% of what is expected for $S=3/2$.

The main role of the “non-magnetic” Co^{3+} ions is to bridge the Co^{2+} ions, providing effective antiferromagnetic coupling. As shown in Fig. 2(c), there are two $\text{Co}^{2+}-\text{O}-\text{Co}^{3+}-\text{O}-\text{Co}^{2+}$ exchange pathways between nearest neighbor (nn) Co^{2+} ions, and one between next-nearest neighbors (nnn). As a result, the spin system appears to be a quasi-two-dimensional square-lattice antiferromagnet with nnn to nn exchange ratio $J_2/J_1 \approx 0.5$; *i.e.*, it is in the critical region where frustration destroys

TABLE I. Anisotropic correlation lengths of the frozen magnetic and charge-orbital order and approximate positions of the corresponding peaks in reciprocal space.

	ξ_{\parallel} (Å)	ξ_{\perp} (Å)	Peak position
charge	28(2)	8.1(7)	$\approx (2h \pm 1, 0, l)$
magnetic	79(3)	10.7(3)	$\approx (2h \pm 0.5, 0, 2l + 1)$

Néel order [16]. This provides a natural explanation for the short spin-spin correlation length in the $a - b$ plane and the peculiar *spin freezing* transition revealed by the temperature dependences shown in Fig. 3. Despite a somewhat “order parameter”-like dependence of the (quasi)elastic magnetic peak intensity, the correlation lengths do not diverge. In fact, the defining feature of the transition is the disappearance of the *energy width* Γ_E of the magnetic scattering, *i.e.* a divergence of the relaxation time for the spin fluctuations [Fig. 3(b)]. Upon appropriate correction for the instrumental resolution, we are able to refine the $\Gamma_E(T)$ dependence down to ~ 0.05 meV. From the power-law fit $\Gamma_E(T) \sim (T - T_{so})^\zeta$ shown in Fig. 3(b) we estimate $\zeta = 2.7(3)$ and $T_{so} \approx 30$ K.

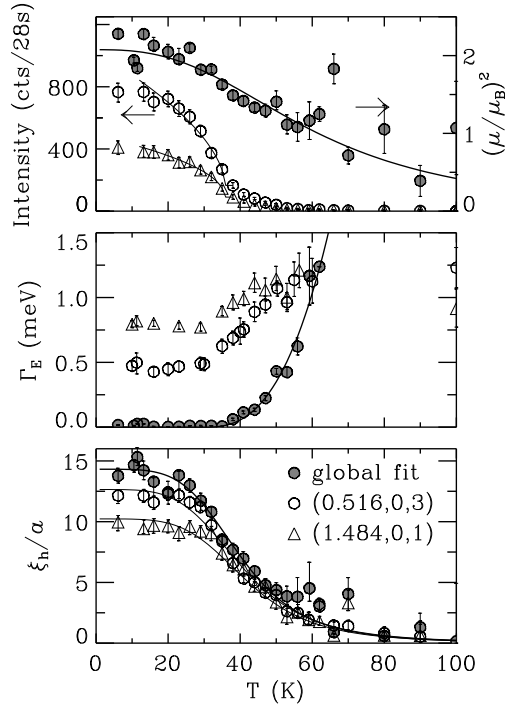


FIG. 3. Temperature dependencies of the parameters of magnetic scattering. Open symbols result from simple fits of the raw data with Lorentzian (a),(c) and Gaussian (b) curves. Shaded circles were obtained from the resolution-corrected global fit of all scans discussed in the text. (a) peak intensity (left scale) and squared magnetic moment per Co site (right scale), (b) energy width, and (c) the in-plane correlation length. Lines in (a),(c) are guides for the eye.

Finally, to underscore the significance of these results we compare the charge and spin order of $\text{La}_{1.5}\text{Sr}_{0.5}\text{CoO}_4$ with that of $\text{La}_{1.5}\text{Sr}_{0.5}\text{MnO}_4$ and other manganates. Firstly, the charge order in $\text{La}_{1.5}\text{Sr}_{0.5}\text{CoO}_4$ occurs independently of the magnetic order, arising at temperatures $\gtrsim 20$ times higher than the characteristic energy scale of the cooperative spin fluctuations. Secondly, compared to the CO in the manganate, it has a much shorter correlation range, $\xi_{co}(\text{Mn})/\xi_{co}(\text{Co}) \gtrsim 10$, but, surprisingly, results in an even stronger charge localization with an acti-

vation behavior of electrical conductivity with $E_a \sim 6000$ K [13]. Thirdly, as a result of the checkerboard order of $\text{Co}^{2+}/\text{Co}^{3+}$ ions and the strong XY anisotropy, the spin system is a stack of weakly interacting square antiferromagnets with nearly critical frustration, $J_2/J_1 \approx 0.5$. In contrast to $\text{La}_{1.5}\text{Sr}_{0.5}\text{MnO}_4$, where simple collinear AFM order occurs, the cobaltate undergoes a freezing transition into a short-range correlated, incommensurate spin-glass state. In fact, this is a rare example where the evolution of the critical spin fluctuations in the course of glassification can be studied by neutron scattering over a dynamic range of about two decades. We intend to further investigate the dynamics of the spin freezing transition in the near future.

We thank NIST Center for neutron Research for hospitality during the experiments. This work was carried out under Contract NO. DE-AC02-98CH10886, Division of materials Sciences, US Department of Energy.

-
- [1] J. M. Tranquada *et al.*, Phys. Rev. Lett. **78**, 338(1997); Phys. Rev. B **59**, 14712 (1999).
 - [2] V. J. Emery, S. A. Kivelson, and O. Zachar, Phys. Rev. B **56**, 6120 (1997); J. Zaanen, Science **286**, 251 (1999).
 - [3] P. Schiffer, A. P. Ramirez, W. Bao and S.-W. Cheong, Phys. Rev. Lett. **75**, 3336 (1995).
 - [4] Y. Murakami *et al.*, Phys. Rev. Lett. **81**, 582 (1998).
 - [5] A. J. Millis, P. B. Littlewood and B. I. Shraiman, Phys. Rev. Lett. **74**, 5144 (1995); A. J. Millis, B. I. Shraiman and R. Mueller, *ibid.* Phys. Rev. Lett. **77**, 175 (1996); A. J. Millis, Phys. Rev. B **53**, 8434 (1996).
 - [6] C. Zener, Phys. Rev. **82**, 403 (1951); P. W. Anderson and H. Hasegawa, Phys. Rev. **100**, 675 (1955).
 - [7] B. J. Sternlieb *et al.*, Phys. Rev. Lett. **76**, 2169 (1996).
 - [8] Y. Murakami *et al.*, Phys. Rev. Lett. **80**, 1932 (1998).
 - [9] M. v. Zimmermann *et al.*, Phys. Rev. Lett. **83**, 4872 (1999); Z. Jirák *et al.*, Phys. Rev. B **61**, 1181 (2000).
 - [10] I. V. Solovyev, K. Terakura, Phys. Rev. Lett. **83**, 2825 (1999); J. v. d. Brink, G. Khaliullin, D. Khomskii, Phys. Rev. Lett. **83**, 5118 (1999).
 - [11] C. N. A. van Duin and J. Zaanen, Phys. Rev. Lett. **80**, 1513 (1998).
 - [12] A. Abragam and B. Bleaney, *Electron Paramagnetic Resonance of Transition Ions* (Dover, New York, 1986), pp. 152-5.
 - [13] Y. Moritomo, K. Higashi, K. Matsuda and A. Nakamura, Phys. Rev. B **55**, R14725 (1997).
 - [14] K. Asai *et al.*, J. Phys. Soc. Jpn. **67**, 290 (1998).
 - [15] M. E. Fisher, Am. J. Phys. **32**, 343 (1964).
 - [16] M. Zhitomirsky, K. Ueda, Phys. Rev. B **54**, 9007 (1996).